

# Prussian Blue

Subjects: [Nanoscience & Nanotechnology](#)

Contributor: Protima Rauwel , Erwan Rauwel

Efficient water remediation methods towards the extraction of  $^{137}\text{Cs}$  are being studied. Prussian blue (PB) and its analogs have shown very high efficiencies in the capture of  $^{137}\text{Cs}^+$  ions.

Prussian blue

$^{137}\text{-Cesium}$

water remediation

magnetic extraction

$^{137}\text{Cs}^+$  selectivity

radioactive contamination

## 1. Prussian Blue

### 1.1. Structure

Prussian blue (PB) is a dark blue pigment synthesized by ferrous ferrocyanide salts with chemical formula  $\text{Fe}_7(\text{CN})_{18}$ . It has a porous structure with the capacity to adsorb the  $^{137}\text{Cs}^+$  ions into its pores and store them there. It is a metal organic framework (MOF) where the inorganic vertices, which donate electrons in the structure, are linked to each other via organic compounds. The complete chemical formula is  $\text{Fe}^{\text{III}}_4[\text{Fe}^{\text{II}}(\text{CN})_6]_3 \cdot x\text{H}_2\text{O}$ . The compound has a face-centered cubic structure (FCC) structure ([Figure 1](#)) belonging to the  $\text{Fm}\bar{3}\text{m}$  space group with a lattice parameter of 10.166 Å. Fe exists in two oxidation states within the structure:  $\text{Fe}^{3+}$  and  $\text{Fe}^{2+}$ . These ions form two different FCC lattices displaced by half a lattice parameter with respect to each other. However, the bi and tri-valent Fe are coordinated differently. Furthermore, they are linked to each other via cyanide groups ( $\text{C} \equiv \text{N}$ ) i.e., C groups are linked to  $\text{Fe}^{2+}$  and N groups to  $\text{Fe}^{3+}$  with high and low spins respectively, in octahedral configurations. The  $\text{Fe}^{2+}$  and  $\text{Fe}^{3+}$  ratio of 3:4 implies that in order to obtain a charge neutrality within the structure a 25% vacancy of  $[\text{Fe}^{+2}(\text{CN})_6]^{4-}$  molecules is necessary [\[1\]](#). Coordinated water molecules occupy the resulting octahedral cavities created by such vacancies; six water molecules are linked to  $\text{Fe}^{2+}$ . The other interstitial water molecules occupy the eight corners of the unit cell ( $\frac{1}{4}, \frac{1}{4}, \frac{1}{4}$ ) and are essential for the insertion of the  $^{137}\text{Cs}^+$  ions in the structure.

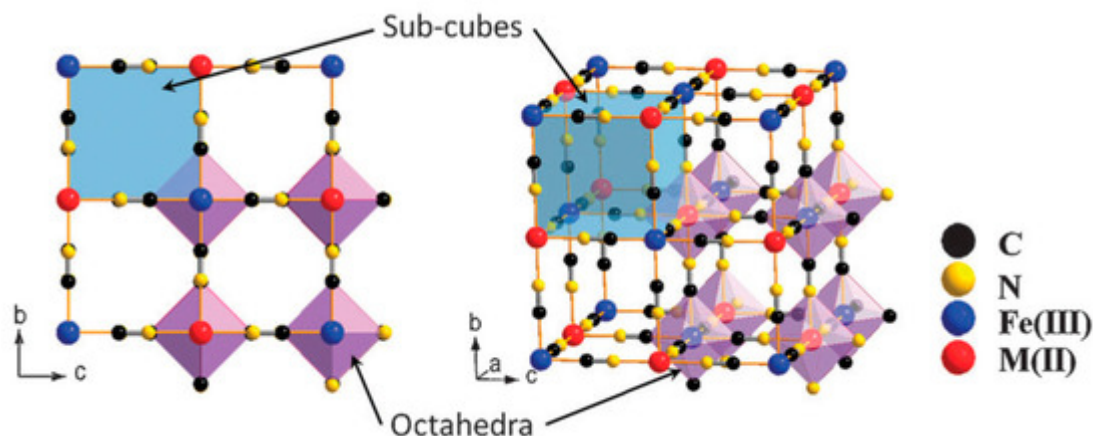


**Figure 1.** Framework of Prussian blue analogues. Adapted with permission from [2], Copyright RSC, 2012.

$\text{Fe}^{+2}$  can be replaced by other transition metals with the same +2 oxidation states such as Ni, Mn, Cu and Co, coordinated exactly like  $\text{Fe}^{+2}$  in the structure and are called PB analogs. However, there are reports of Cd and Zn with slightly larger atomic radii also being incorporated into the structure owing to their +2 oxidation state [3]. The aim in including different species into the structure is to provoke a distortion of the PB lattice by producing vacancies of the high spin state molecule along with distortions in the vacant cages, in order to facilitate the capture and sequestration of the  $^{137}\text{Cs}^+$  [4].

## 1.2. $^{137}\text{Cs}^+$ Ion Capture Mechanism in Prussian Blue

The compound is insoluble in water and the basic mechanism consists of ion exchange of  $^{137}\text{Cs}^+$  and  $\text{H}^+$  with the former occupying hydrophilic vacancies [5]. PB analogs have very different mechanisms of ion exchange or capture depending upon the anionic and alkali metal cation concentrations. Since PB and its analogs contain large amounts of interstitial and coordinated water,  $^{137}\text{Cs}^+$  is captured by a defect created by a  $[\text{Fe}^{+2}(\text{CN})_6]$  vacancy, which creates a spherical cavity whose size is equivalent to the hydration radius of  $^{137}\text{Cs}^+$ . Nevertheless, recent calculations have demonstrated that a completely dehydrated  $^{137}\text{Cs}^+$  ion can be incorporated into the structure with the release of a water molecule from the interstitial sites [6]. This is similar to certain clays, where on dehydrating the interlayers the  $^{137}\text{Cs}^+$  selectivity increases [7]. On the other hand, water soluble analogs such as metal hexacyanoferrates (HCF) consisting of an alkali metal cation with a  $[\text{Fe}^{+2}(\text{CN})_6]$  anion, used for the extraction of  $^{137}\text{Cs}^+$  have shown less efficiency. In such compounds  $\text{Na}^+$  or  $\text{K}^+$  are incorporated during the synthesis of the MOF in order to render them water-soluble [8]. In addition to  $^{137}\text{Cs}^+$  capture mechanisms for non-soluble analogs; the water-soluble analogs mainly depend on the  $\text{Na}^+$  or  $\text{K}^+$  ion exchanges with  $\text{Cs}^+$ . Takahashi et al., have studied the  $^{137}\text{Cs}^+$  uptake in  $\text{KCuHCF}$  PB analog in order to understand their lower adsorption capacity [8]. Three main mechanisms governed the  $^{137}\text{Cs}^+$  ion exchange according to them, with the  $^{137}\text{Cs}^+$ - $\text{K}^+$  ion exchanges being predominant, as also stipulated by other research groups. In case of low anionic vacancies, the percolation of  $^{137}\text{Cs}^+$  through the vacancies was prevalent. Finally, for low  $\text{K}^+$  incorporation in the structure, proton exchange between  $^{137}\text{Cs}^+$  and  $\text{K}^+$  ions was evidenced. Ayrault et al., report a degradation in the crystal structure of the  $\text{KCuHF}$  soluble compound after  $^{137}\text{Cs}^+$  adsorption which was not observed in the non-soluble counterpart [9].

### 1.3. Nanostructured Prussian Blue

$^{137}\text{Cs}^+$  adsorption in PB crystals is a very slow process. Fujita et al., have demonstrated that after two weeks of adsorption experiments, the depth of  $^{137}\text{Cs}^+$  adsorption was at most between 1–2 nm, irrespective of the crystal size [10]. This implies that most of the adsorption occurs on the surface of the crystallites. This low diffusion depth is mainly attributed to the blocking of the vacancies by captured  $^{137}\text{Cs}^+$  ions, which in turn hinders further  $^{137}\text{Cs}^+$  diffusion. Since the diffusion depth appears to be a constant, increasing the specific surface would therefore be a solution to increasing the  $^{137}\text{Cs}^+$  uptake. One way of augmenting the specific surface is by synthesizing nanoparticles of PB. The surface to volume ratio of crystallites increases as their size decreases; therefore nanoparticles have an extremely large surface to volume ratio. For example, a 3 nm nanoparticle will have 50% of its atoms on its surface. This would also imply that in the case of PB nanocrystals most of the vacancies and sites responsible for  $^{137}\text{Cs}^+$  adsorption would be available on the surface, thus enhancing its specific surface. To this end, different research groups have produced various PB analogs of type Metal(M)-Co, where the nature of M defines the efficiency of the uptake. Liu et al., have demonstrated that Zn assisted Fe-Co PB analogs present high  $^{137}\text{Cs}^+$  uptake efficiency [11]. They also observed that the size of the PB analog particle reduced with the reduction of Fe in the structure; for pure Zn-Co analogs, a crystallite size of ~73 nm was calculated, displaying the highest  $^{137}\text{Cs}^+$  adsorption as depicted in Figure 2.

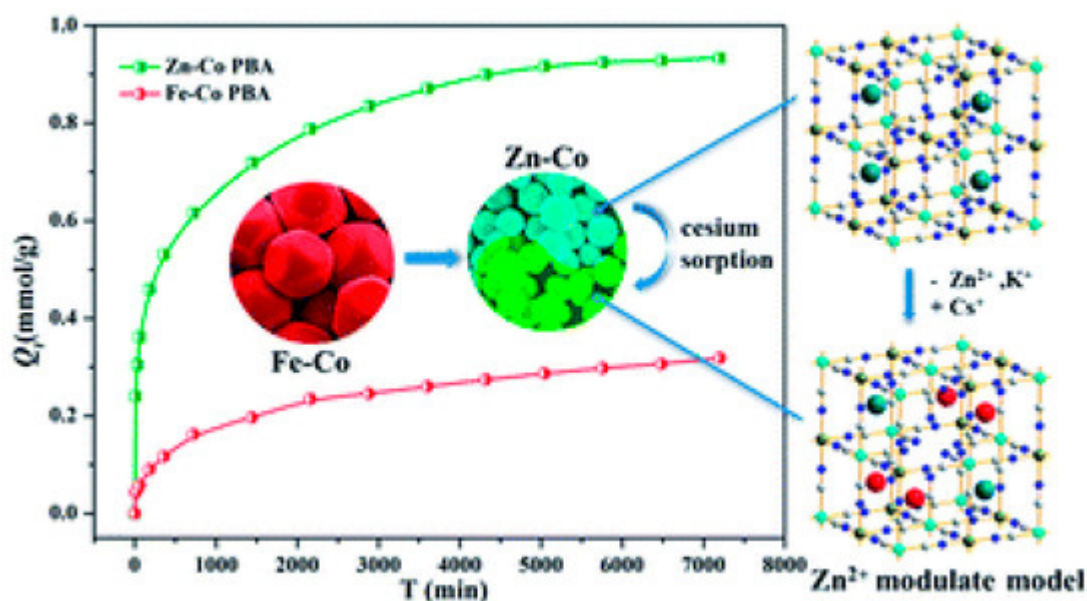


**Figure 2.** Adsorption efficiency of Fe-Co and Zn-Co prussian blue (PB) analogs as a function of time. The Zn-Co PB analog exhibits a higher  $Q_t$  ( $Q_t$  is the adsorption capacity per unit gram of the sorbent at a given time  $t$ ) owing to the reduction in size of the nanoparticles. Adapted from [11] under the Creative Commons agreement from RSC, 2017.

Considering that the  $^{137}\text{Cs}^+$  adsorption depth is only about 1–2 nm, hollow PB nanoparticles may offer many more advantages. They not only have a very active surface area due to their large surface to volume ratio but their hollow interior is also capable of capturing and storing  $^{137}\text{Cs}^+$  [12]. A surfactant polyvinylpyrrolidone (PVP) was used

to stabilize the nanoparticle and increase their dispersion in aqueous solutions. [Figure 3](#) compares the efficiency of solid and hollow PB cubes of  $\sim 200$  nm, in the capture of  $^{137}\text{Cs}^+$ . The elemental mapping of [Figure 3B](#) depicts a higher concentration of captured  $^{137}\text{Cs}^+$  ions within the hollow structures than the filled ones in [Figure 3A](#). Nevertheless,  $^{137}\text{Cs}^+$  diffusion depth greater than 2 nm would require higher activation energy at room temperature. Other methods are required to determine the exact diffusion depth in such structures, as these results are mainly qualitative. Besides, it is well known that the use of a surfactant shields the active sites and prevents the capture of  $^{137}\text{Cs}^+$ . In order to avoid such shielding effects, PB could be coated onto support materials instead through hydroxyl bonds that anchor the PB to the support material. Carboxylic groups also tend to immobilize the PB particles in a sturdier manner. Wi et al., used a polyvinyl support surface functionalized with acrylic acid. This allowed converting the OH groups to COOH and providing a better adhesion of the PB [\[13\]](#). The PB nanoparticles were immobilized on the PVP sponge and an increase in  $^{137}\text{Cs}^+$  uptake efficiency by five times was reported, compared to the hydroxyl bond functionalization.

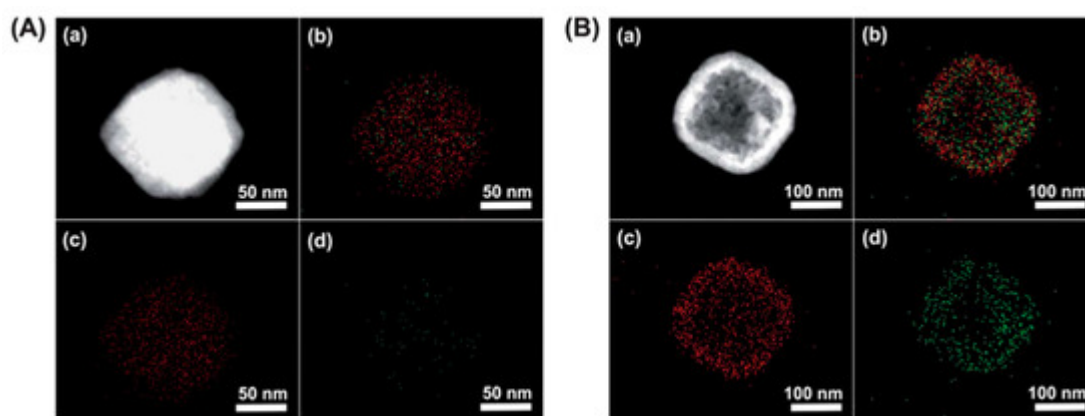


**Figure 3.** Elemental mapping images of solid (A) and hollow PB (B) nanoparticles of 190 nm in diameter. (a) Dark-field TEM image, (b) elemental mapping of both Fe and Cs (c) elemental mapping of Fe, and (d) elemental mapping of Cs. Adapted with permission from [\[12\]](#), Copyright RSC, 2012.

## 2. Magnetic Extraction Using Prussian Blue

There are reports of photo-induced magnetism where an electromagnetic radiation induces a residual magnetization even after the excitation is turned off, [\[14\]](#) due to low and high spin combinations of the transition metals in PB analogs. On their own, PB and its analogs exhibit ferromagnetism at a Curie temperature of 11 K with a saturation magnetization of 3.4 emu/g as obtained by Tokoro et al., for Mn-Rb-Fe PB analogs [\[15\]](#). The presence of Mn in the structure creates a Jahn-Teller distortion [\[16\]](#) by changing the M-CN-M bond angle and deviating it from  $180^\circ$ , whereupon inducing ferromagnetism. Among the various PB analogs, Mn based ones have shown the highest saturation magnetization [\[17\]](#). One method of decreasing the Curie temperature of PB is by synthesizing nanoparticles of PB. Uemura et al., have demonstrated a decrease in  $T_c$  from 5.5 K in bulk PB to 4 K for PB nanoparticles protected by PVP [\[18\]](#). Nevertheless, finding practical applications involving magnetic extraction would require having a  $T_c$  at around room temperature. Also, humidity increases the Curie temperature for Co-Cr

PB analogs, [15] thus making it difficult for their direct application in aqueous media. This implies that most methods using PB for  $^{137}\text{Cs}^+$  extraction, do not prescribe any efficient approach to recover the exhausted adsorbent.

Literature on nanostructured PB alone is very scarce as they are generally combined with magnetic nanomaterials like superparamagnetic iron oxide nanoparticles (SPIONs) i.e.,  $\text{Fe}_3\text{O}_4$  or  $\gamma\text{-Fe}_2\text{O}_3$  nanoparticles. In the past, there have been reviews briefly describing  $^{137}\text{Cs}^+$  adsorption employing magnetic PB- $\text{Fe}_3\text{O}_4$  nanoparticles [19]. In nanostructures, physical properties such as magnetic moment as well as adsorption vary as a function of the nanoparticle size and further depend upon the surfactants used to stabilize them during synthesis. In the paragraph that follows, the efficiency of magnetic PB nanoparticles and their combination with magnetic nanoparticles is assessed.

Core-shell structures with the magnetite constituting the core and the PB active layer constituting the shell have been employed. Jang et al., have reported that the poly(diallyldimethylammoniumchloride) (PDDA)@Iron oxide nanoparticles can act as nucleation sites for the precipitated PB, resulting in the coating of a negatively charged PB on the PDDA@Iron oxide nanoparticle surface [20]. Furthermore, they have also studied the magnetic properties of  $\text{Fe}_3\text{O}_4$  and have observed a decrease in the saturation magnetization from 56 emu/g for pure  $\text{Fe}_3\text{O}_4$  to 12 emu/g for the PB- $\text{Fe}_3\text{O}_4$  nanocomposite. The reduction was mostly due to the shielding of the superparamagnetism of  $\text{Fe}_3\text{O}_4$  by the PB capping. Nevertheless, successful magnetic extraction was achieved with the nanocomposite [21]. PB analog compounds tend to show degradation in various applications after successive cycles of reuse. Chang et al., Figure 4A, have synthesized  $\text{Fe}_3\text{O}_4$  (shell)-PB (core) nanocomposites with sizes between 20–40 nm; [22] two different concentrations of  $\text{FeCl}_3$  were used during the synthesis. The higher Fe concentrations produced  $\text{Fe}_3\text{O}_4$  cores with a higher magnetic saturation moment (Figure 4B), which conversely had an adverse effect on the  $^{137}\text{Cs}^+$  adsorption due to the higher shielding of the active sites in the PB core as depicted in Figure 4C.

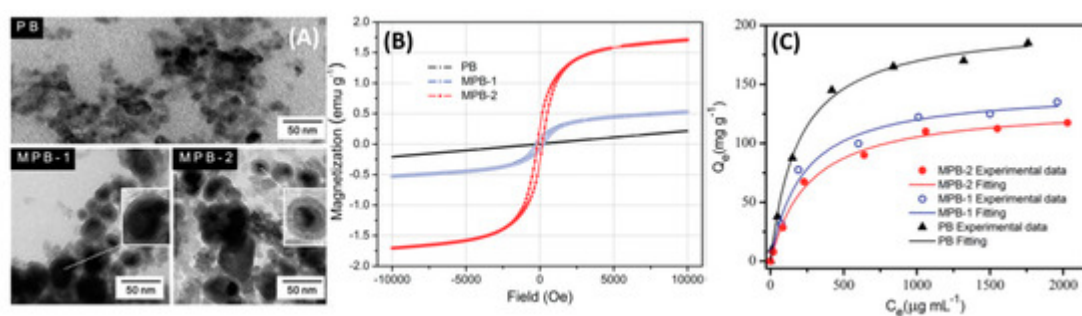


**Figure 4.** (A) TEM images of PB and magnetic PB (MPB) nanoparticles. (B) Field-dependent magnetization of PB and magnetic PB nanoparticles. (C) Adsorption capacity of samples under different  $\text{Cs}^+$  concentration.  $T = 25\text{ }^\circ\text{C}$ ; contact time = 6 h;  $[\text{Cs}^+]_{\text{initial}} = 50\text{--}2500\text{ }\mu\text{g/mL}$ ;  $m_{\text{adsorbent}}/V_{\text{solution}} = 4\text{ }\mu\text{g/mL}$ . Adapted with permission from [22], Copyright RSC, 2016.

Some researchers have also used different ferrimagnetic nanoparticles like  $\text{CoFe}_2\text{O}_4$  combined with PB for the extraction of cesium and have indicated very high efficiencies compared to pure  $\text{CoFe}_2\text{O}_4$ , which has some interesting  $^{137}\text{Cs}^+$  adsorption capacity by itself [23].  $\text{CoFe}_2\text{O}_4$  possesses the spinel structure and tends to be

physically more robust but is a hard magnetic compound compared to  $\text{Fe}_3\text{O}_4$ . The latter is a soft magnet with a very small residual magnetization and can therefore be used in successive cycles of extraction.

## References

1. Kumar, A.; Yusuf, S.M.; Keller, L. Structural and magnetic properties of  $\text{Fe}[\text{Fe}(\text{CN})_6]\cdot 4\text{H}_2\text{O}$ . *Phys. Rev. B* 2005, 71, 054414.
2. Lu, Y.; Wang, L.; Cheng, J.; Goodenough, J.B. Prussian blue: A new framework of electrode materials for sodium batteries. *Chem. Commun.* 2012, 48, 6544–6546.
3. Nie, P.; Shen, L.; Luo, H.; Ding, B.; Xu, G.; Wang, J.; Zhang, X. Prussian blue analogues: A new class of anode materials for lithium ion batteries. *J. Mater. Chem. A* 2014, 2, 5852–5857.
4. Matsuda, T.; Kim, J.; Moritomo, Y. Control of the alkali cation alignment in Prussian blue framework. *Dalton Trans.* 2012, 41, 7620–7623.
5. Ishizaki, M.; Akiba, S.; Ohtani, A.; Hoshi, Y.; Ono, K.; Matsuba, M.; Togashi, T.; Kananizuka, K.; Sakamoto, M.; Takahashi, A.; et al. Proton-exchange mechanism of specific  $\text{Cs}^+$  adsorption via lattice defect sites of Prussian blue filled with coordination and crystallization water molecules. *Dalton Trans.* 2013, 42, 16049–16055.
6. Ruankaew, N.; Yoshida, N.; Watanabe, Y.; Nakano, H.; Phongphanphanee, S. Size-dependent adsorption sites in a Prussian blue nanoparticle: A 3D-RISM study. *Chem. Phys. Lett.* 2017, 684, 117–125.
7. Eberl, D.D. Alkali Cation Selectivity and Fixation by Clay Minerals. *Clays Clay Miner.* 1980, 28, 161–172.
8. Takahashi, A.; Tanaka, H.; Minami, K.; Noda, K.; Ishizaki, M.; Kurihara, M.; Ogawa, H.; Kawamoto, T. Unveiling  $\text{Cs}^+$ -adsorption mechanism of Prussian blue analogs:  $\text{Cs}^+$ -percolation via vacancies to complete dehydrated state. *RSC Adv.* 2018, 8, 34808–34816.
9. Ayrault, S.; Jimenez, B.; Garnier, E.; Fedoroff, M.; Jones, D.J.; Loos-Neskovic, C. Sorption Mechanisms of Cesium on  $\text{CuI}_2\text{FeII}(\text{CN})_6$  and  $\text{CuI}_3[\text{FeIII}(\text{CN})_6]_2$  Hexacyanoferrates and Their Relation to the Crystalline Structure. *J. Solid State Chem.* 1998, 141, 475–485.
10. Fujita, H.; Miyajima, R.; Sakoda, A.J.A. Limitation of adsorptive penetration of cesium into Prussian blue crystallite. *Adsorption* 2015, 21, 195–204.
11. Liu, J.; Li, X.; Rykov, A.I.; Fan, Q.; Xu, W.; Cong, W.; Jin, C.; Tang, H.; Zhu, K.; Ganeshraja, A.S.; et al. Zinc-modulated Fe–Co Prussian blue analogues with well-controlled morphologies for the efficient sorption of cesium. *J. Mater. Chem. A* 2017, 5, 3284–3292.

12. Torad, N.L.; Hu, M.; Imura, M.; Naito, M.; Yamauchi, Y. Large Cs adsorption capability of nanostructured Prussian Blue particles with high accessible surface areas. *J. Mater. Chem.* 2012, 22, 18261–18267.
13. Wi, H.; Kang, S.-W.; Hwang, Y. Immobilization of Prussian blue nanoparticles in acrylic acid-surface functionalized poly(vinyl alcohol) sponges for cesium adsorption. *Environ. Eng. Res.* 2019, 24, 173–179.
14. Pajeroski, D.M.; Gardner, J.E.; Frye, F.A.; Andrus, M.J.; Dumont, M.F.; Knowles, E.S.; Meisel, M.W.; Talham, D.R. Photoinduced Magnetism in a Series of Prussian Blue Analogue Heterostructures. *Chem. Mater.* 2011, 23, 3045–3053.
15. Tokoro, H.; Ohkoshi, S.-I. Novel magnetic functionalities of Prussian blue analogs. *Dalton Trans.* 2011, 40, 6825–6833.
16. Buzin, E.R.; Prellier, W.; Mercey, B.; Simon, C.; Raveau, B. Relations between structural distortions and transport properties in Nd<sub>0.5</sub>Ca<sub>0.5</sub>MnO<sub>3</sub> strained thin films. *J. Phys. Condens. Matter* 2002, 14, 3951–3958.
17. Nakotte, H.; Shrestha, M.; Adak, S.; Boergert, M.; Zapf, V.S.; Harrison, N.; King, G.; Daemen, L.L. Magnetic properties of some transition-metal Prussian Blue Analogs with composition M<sub>3</sub>[M'(C,N)<sub>6</sub>]·2·xH<sub>2</sub>O. *J. Sci. Adv. Mater. Devices* 2016, 1, 113–120.
18. Uemura, T.; Kitagawa, S. Prussian Blue Nanoparticles Protected by Poly(vinylpyrrolidone). *J. Am. Chem. Soc.* 2003, 125, 7814–7815.
19. Liu, X.; Chen, G.-R.; Lee, D.-J.; Kawamoto, T.; Tanaka, H.; Chen, M.-L.; Luo, Y.-K. Adsorption removal of cesium from drinking waters: A mini review on use of biosorbents and other adsorbents. *Bioresour. Technol.* 2014, 160, 142–149.
20. Jang, S.-C.; Kang, S.-M.; Kim, G.Y.; Rethinasabapathy, M.; Haldorai, Y.; Lee, I.; Han, Y.-K.; Renshaw, J.C.; Roh, C.; Huh, Y.S. Versatile Poly(Diallyl Dimethyl Ammonium Chloride)-Layered Nanocomposites for Removal of Cesium in Water Purification. *Materials* 2018, 11, 998.
21. Jang, J.; Lee, D.S. Magnetic Prussian Blue Nanocomposites for Effective Cesium Removal from Aqueous Solution. *Ind. Eng. Chem. Res.* 2016, 55, 3852–3860.
22. Chang, L.; Chang, S.; Chen, W.; Han, W.; Li, Z.; Zhang, Z.; Dai, Y.; Chen, D. Facile one-pot synthesis of magnetic Prussian blue core/shell nanoparticles for radioactive cesium removal. *RSC Adv.* 2016, 6, 96223–96228.
23. Hassan, M.R.; Aly, M.I. Adsorptive removal of cesium ions from aqueous solutions using synthesized Prussian blue/magnetic cobalt ferrite nanoparticles. *Part. Sci. Technol.* 2019, 1–11.

---

Retrieved from <https://encyclopedia.pub/entry/history/show/25089>